Thermal analysis of friction stir welded joint for 304l stainless steel material using ansys Mechanical APDL

Sumit Kumar, Ravi Kumar, Lokesh Joshi

ABSTRACT: A simple three-dimensional nonlinear thermal and thermomechanical model for friction stir welding (FSW) is presented with the help of ANSYS 14.5. The amount of heat generated between the shoulder and the work piece during friction stir processing dictates the quality of the processed zone. Hence understanding the distribution of heat and obtaining the temperature contours will assist in understanding the general process of friction stir processing. FSW simulation is performed for tool rotational speed on 250 and 400 rpm and they allow partial sliding between the shoulder and the work piece. The numerical analysis presents that the temperature field in the FSW process is symmetrically distributed with respect to the welding line. The main objective is to study the variation of temperature on surface and HAZ in a friction stir welded plate of 304L stainless steel. Boundary conditions in the thermal modeling of process also play a vital role in the final temperature profile. Virtual experimental data of this present study illustrates that peak temperatures are higher on the advancing side than the retreating side during weld process.

Keywords: FSW, 304L stainless steel, HAZ, Thermal modeling.

1 INTRODUCTION

Friction Stir Welding (FSW) was invented by Wayne Thomas at TWI (The Welding Institute), and the first patent applications were filed in the UK in December 1991[1-5]. This process is fast, efficient and capable of producing defect free joints, versatile and environment friendly. As compared to the conventional welding, FSW consumes considerably less energy. No cover gas or flux is used, thereby making the process environmentally friendly [6]. The process of friction stir welding is based on friction heating at the facing surfaces of two sheets to be joined in the FSW process a special tool with a properly designed rotating probe along the contacting metal plates produces a highly plastically deformed zone by the stirring action. The parts have to be securely clamped to prevent the joint faces from being forced apart. Frictional heat between the wear resistant welding tool and the workpieces causes the latter to soften without reaching melting point, allowing the tool to traverse along the weld line. The side on which the tool rotation is parallel to the weld direction is called advancing side and the side on which the tool rotation is opposite to the weld direction is called retreating side. The original applications for friction stir welding are the welding of long lengths of material in the aerospace, shipbuilding and railway industries. Examples include large fuel tanks and other containers for space launch vehicles, cargo decks for high speed ferries, and roofs for railway carriages [7].

- Sumit Kumar, Masters degree program in Thermal engineering in *Bipin Tripathi Kumaon Institute of Technology, Dwarahat, Almora* Uttrakhand, India, PH-9997794595. E-mail: sumitkumar1991@outlook.com
- *Ravi Kumar, Assistant Professor* ,Department of Mechanical Engineering in *Bipin Tripathi Kumaon Institute of Technology, Dwarahat, Almora* Uttrakhand, India

This novel technology is one of the first to successfully join the notoriously difficult to weld 7xxx and 2xxx series alloys, producing quick, energy efficient [7]. Tang et al. [8] presented the experimentally measured temperature distributions of the work piece in FSW Gould and Feng [9] proposed a simple heat transfer model for predicting the temperature distribution in the workpiece of the FSW. Chao and Qi [10,11] developed a moving heat source model in a finite element analysis and simulated the transient temperature of the FSW process. Colegrove et al. [12] and Frigaard et al. [13] developed three-dimensional heat flow models for the prediction of temperature fields in the FSW. A demonstration of the tremendous potential and successful applications of aluminum FSW in airframe structures can be found in Talwar et al. [14].

To further understand the fundamental mechanisms associated with the welding formation process and improve the welding quality for the FSW of steels, numerical modeling and simulations of transient temperature are valuable and necessarily needed.

2. THERMOMECHANICAL MODEL

2.1 Kinematic assumptions -The heat generated at the pin is approximately two percent (2%) of the total heat so therefore tool pin is ignored [15, 16]. In the simulation welds two 304L stainless steel plates (work piece) with a cylindrical shape tool is used in this present work. The welding zone is divided into three parts defined as the flow arm zone for the torsion velocity field, the stirring zone for the "vortex like" velocity field, and the rest of the sheet. All three zones undergo the circumventive velocity field [18].

2.2 Circumventive velocity field

This field describes material flow around the pin like water around a bridge pile [18].

$$\vec{V} = \begin{bmatrix} U_r = v_\infty \left(1 - \frac{r_0^2}{r^2}\right) \cos\theta \\ U_\infty = -v_\infty \left(1 + \frac{r_0^2}{r^2}\right) \sin\theta - \frac{\Gamma}{2\pi r} \\ U_z = 0 \end{bmatrix} \quad (1)$$

Where r_0 is the pin radius, r is the distance to the tool axis and v_∞ (m/s) is the welding velocity. The material circulation Γis added to account for partial circumferential dragging of the material due to the rotation of the tool. The angular velocity (s^{-1}) of the material dragged by the pin surface.

2.3 Torsion velocity field

Since friction occurs between the shoulder of the tool and the upper surface of the workpiece, it develops a shear strain under the surface. Therefore, a torsion velocity field (centered on the probe axis) is introduced to describe this shearing effect in the flow arm zone [18].

$$\vec{V} = \begin{bmatrix} U_\theta = r\Omega_{surf} \frac{z - z_{flowarm}}{z_{surf} - z_{floearm}} \\ U_r = 0 \\ U_z = 0 \end{bmatrix} \quad (2)$$

Ref. [12] stated that the numerical welding simulation requires a wide range of material properties as input data. Considering the temperature field calculation, the thermophysical properties i.e. density, specific heat capacity and thermal conductivity λ are needed. For the calculation of the distortions and stresses, the thermomechanical properties i.e. yield strength, hardening behavior, Young's modulus, thermal expansion and Poisson's ratio are a prerequisite. Calculation of the thermal conductivity as input for the simulation has been suggested by the equation:

$$\lambda(T) = a(T).\ \varrho(T).\ Cp(T) \quad (3)$$

The tensile strain calculation has been suggested using thermal expansion coefficient at room temperature as:

$$\varepsilon = \alpha RT(\Delta T/\Delta t \quad (4)$$

The governing continuity equations for the material flow are given [19]

$$\rho \frac{\partial u_i u_j}{\partial x_i} = -\frac{\partial p}{\partial x_i} + \frac{\partial}{\partial x_i}\left(\eta \frac{\partial u_j}{\partial x_i} + \eta \frac{\partial u_i}{\partial x_j}\right) - \rho u_{weld} \frac{\partial u_j}{\partial x_j} \quad (5)$$

$$\frac{\partial u_i}{\partial x_i} = 0 \quad (6)$$

2.4 Heat generation from the shoulder surface

The heat generation from this segment is [20]

$$dQ = \omega \cdot r \cdot dF = \omega \cdot r^2\ \tau_{contact} \cdot d\theta \cdot dr \quad (7)$$

Where r is the distance from the considered area to the center of rotation, ω is the angular velocity, and r·d and dr are the segment dimensions. Integration of Eq. (7) over the shoulder area from R_{PT} to $R_{shoulder}$ gives the shoulder heat generation Q_1.

$$Q_1 = \int_0^{2\pi} \int_{R_{PS}}^{R_{shoulder}} \omega \cdot r^2\ \tau_{contact}.d\theta\ .dr \quad (8)$$

$$Q_1 = \frac{2}{3}\ \pi\omega\tau_{contact}(R^3{}_{shoulder} - R^3{}_{PS}) \quad (9)$$

3. BOUNDARY CONDITIONS

(a) Tool shoulder/workpiece interface: - The heat flux boundary condition for the workpiece at the tool shoulder and workpiece interface is

$$k\frac{\partial T}{\partial n} = q_s \quad (10)$$

(b) Tool pin/workpiece interface: - The heat flux boundary condition at the tool pin and workpiece interface is similar to the tool shoulder/workpiece interface, and can be written as

$$k\frac{\partial T}{\partial n} = q_p \quad (11)$$

(C) The convection boundary conditions: - The convection boundary condition for all the workpiece surfaces exposed to the air can be expressed as

$$k\frac{\partial T}{\partial n} = h(T - T_0) \quad (12)$$

Where n is the normal direction vector of boundary and h is the convection coefficient. The surface of the workpiece in contact with the backup plate is simplified to the convection condition with an effective convection coefficient in this model.

4. INITIAL CONDITION

The initial condition for the calculation is:

$$T(x, y, z, 0) = T_i \quad (13)$$

5. NUMERICAL SOLUTION:-

In the present study, the modeling and analysis of FSW process for 304L stainless steel butt weld is carried out using the finite element based software, ANSYS MECHANICAL APDL (Virtual experiment software module). Steady thermal finite element analysis is performed in order to obtain the temperature distribution in the welded steel plate during the welding operation. Three-dimensional model is developed to carry out parametric study of friction stir welded joint on variation of process parameter such as tool rotational speed.

6. PROCESS METHODOLOGY

The virtual experimental work is completed using Ansys's Mechanical APDL 14.5 friction stir welding. The work materials employed in the present study was the 304L stainless steel, measuring 3 mm for thickness, 73 mm for length and 32 mm for width the butt joint configuration was modeled. The Methodology of the experimental work in explained through block diagram as shown in fig.1

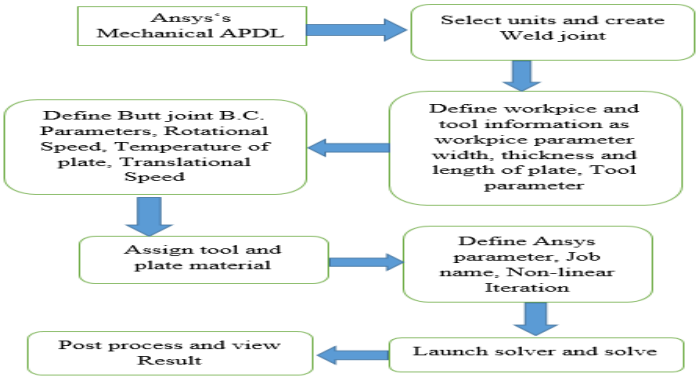

Fig. 1 Process flow chart

The Friction stir weld- tool was considered made from Polycrystalline Cubic Boron Nitride (PCBN) material. The shoulder diameter (d) and length (l) are 16 mm and 25 mm respectively. The welding speed is kept constant for both all experiments as 1.8 mm/s whereas the tool rotation speed was 250 and 400 rpm.

7. RESULTS & DISCUSSION

The FEA mesh is which has 6 layers of elements in the thickness direction and brick solid elements and 5081 nodes and 2503 Element in thermo-mechanical analyses. Fine FEA mesh is used in this current work that may generate nearly identical results, but the computational time increased significantly [21]. APDL (ANSYS Parametric Design Language) code is developed for transient thermal analyses. Transient thermal finite element analyses are performed in order to obtain the temperature distribution in the welded steel plates during the welding operation. Figures 5 and 6 show the temperature profiles in the work piece during the welding operation for ω=400 rev/min and 250 rev/min for v= 3 mm/s.Temperature distribution Contours obtained from the virtual experiment work for tool rotational speeds are summarized in graphs for the maximum or peak temperature in HAZ of weld joint. All frictional dissipated energy is converted into heat during load step. The heat is generated at the tool-work piece interface. Most of the heat is transferred to the work piece.

7.1 Temperature distribution contours for different tool rotational speed:-

As a result, the temperature of the workpiece increases rapidly compared to that of the tool. The heat transfer process during the tool penetration period cannot be modeled if the heat input from the pin is not included.

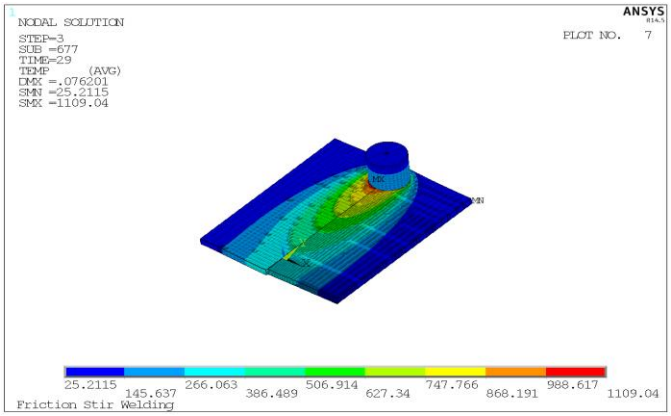

Fig. 2 Temperature distribution contours for 400 rpm tool rotational speed respectively

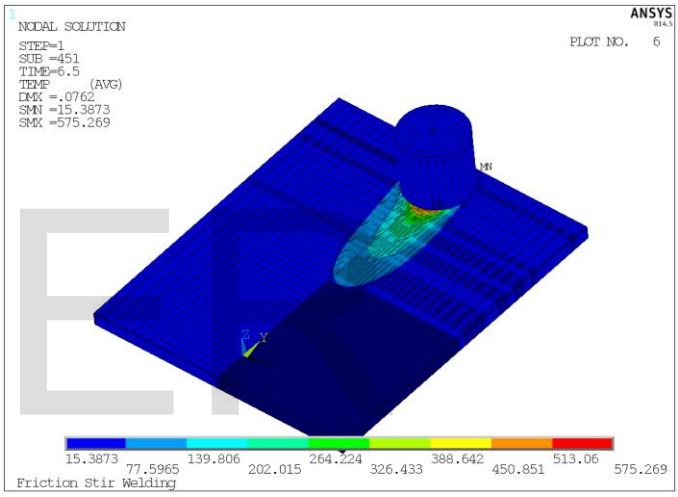

Fig. 3 Temperature distribution contours for 250 rpm tool rotational speed respectively

Moreover, the initial field is very important in a transient heat transfer model, especially for modeling the preheat effects of laser-assisted preheated FSW [22]. For this purpose, the heat transfer during the tool penetration period cannot be neglected. Fig. 7, 8 shows the calculated temperature contours of the peak temperatures of the welding cross section. The value of the calculated peak temperature in the nugget is about 590 ^{0}C at 250 rpm, the calculated peak temperature of the TMAZ is in the range of 481 to 512 ^{0}C and the calculated peak temperature in the HAZ is in the range of 512 to 449 ^{0}C.

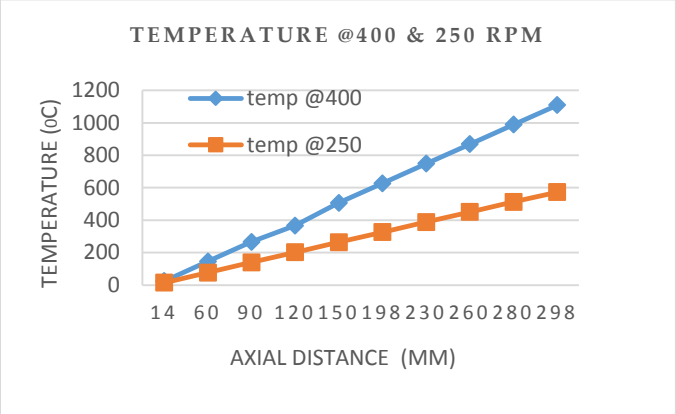

Fig. 4 Plot of variation of Temperature at 250 rpm and 400 rpm.

The value of the peak temperature at 400 rpm in nugget is about 1109 ^{0}Cand the calculated peak temperature of TMAZ is in rang of 890 to 1000 ^{0}C and the peak temperature in HAZ is in rang of 750 to 910 ^{0}C.

7.2 Stress distribution contours for different tool rotational speed: -

As in welding, the primary stress in FSW occurs in the weld and is in the longitudinal or weld-line direction. The variations of the longitudinal stress along the transverse direction at the middle section of workpiece are shown in Fig. 9 for the rotational speed of 250 and 400 rpm, respectively.

It is observed from these figures that (a) the stresses along the transverse section for the rotational speed of 250 and 400 rpm are very close to each other. (b) The numerical results of longitudinal stresses reveal small difference between the top surface of these thin welded plates for both rotation speed 250 & 400 rpm.

The maximum stress develop in weld line is 528043 Pa. All other calculated stresses, including the ones in the transverse and thickness directions, are very small and close to zero. They are not reported here because of its less importance.

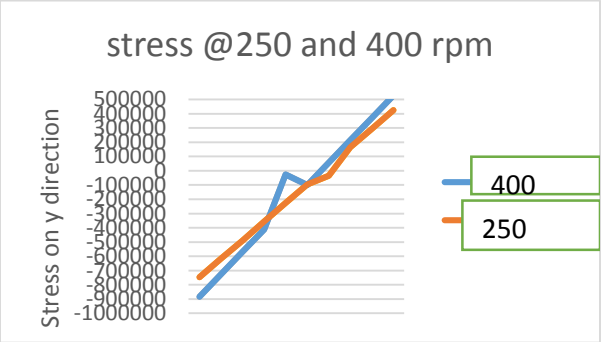

Fig. 5 Plot of variation of Stress on weld line at 90 mm axial (y) direction both 250 & 400 rpm

7.3 Temperature gradient distribution contours for different tool rotational speed:-

Heat transfer simulations are performed for the FSW of 304L stainless steel. Only the last or the final numerical results are reported here. The frictional and heat generated during the FSW process propagates rapidly into remote regions of the plates. On the top and side surfaces of the work piece, convection and radiation account for heat loss to the ambient [24]. Conduction losses also occur from the bottom surface of the work piece to the backing plate. Available data suggest

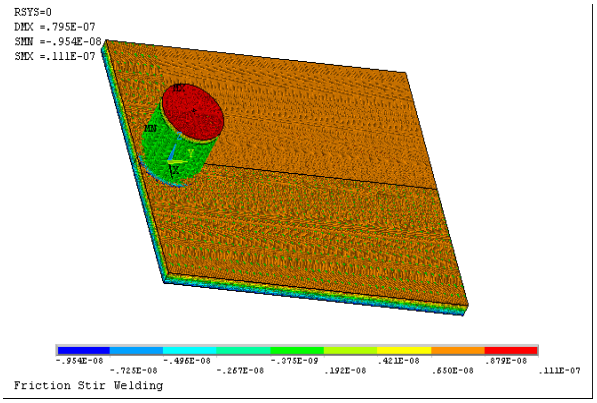

Fig. 6 Temperature gradient on load step 1 at 400 rpm

that the value of the convection coefficient lies between 10 and 30 W/m^2 °C [23,24,25] for the work piece surfaces, except for the bottom surface. The value of the convection coefficient is 30 W/m^2°C for work piece and tool.

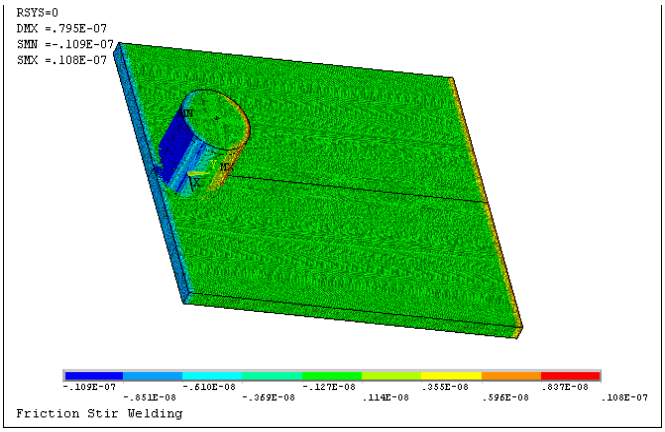

Fig. 7 Temperature gradient on load step 1 at 250 rpm

This coefficient affects the output temperature. A lower coefficient increases the output temperature of the model. A high overall heat-transfer coefficient is 280 W/m^2 °C is assumed for the conductive heat loss through the bottom surface of the workpiece. As a result, the bottom surface of the workpiece is also treated as a convection surface for modeling conduction losses. Because the percentage of heat lost due to radiation is

low, radiation heat losses are ignored. An initial temperature of 25 °C is applied on the model. Temperature boundary conditions are not imposed anywhere on the model.

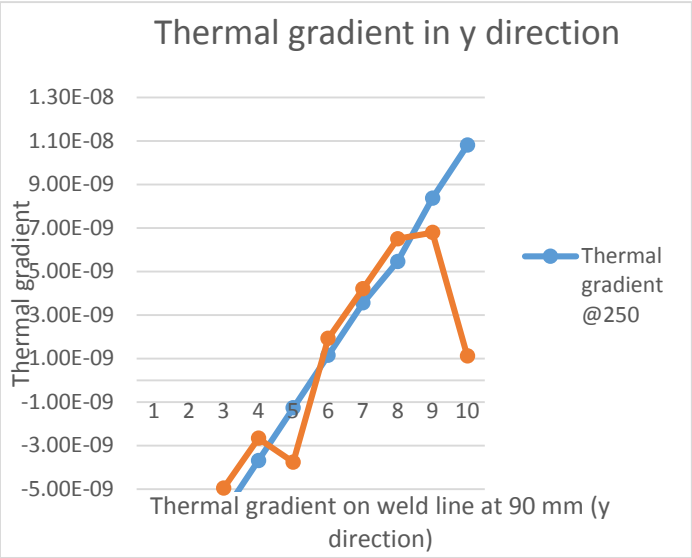

Fig. 8 Plot of variation of Thermal gradient on weld line at 90 mm y direction

7.4 Penetration period: -During this period, the rotating tool pin penetrates into the workpiece, until the tool shoulder contacts the workpiece. The penetration speed is chosen to be 3 mm/s in the calculation, and the corresponding penetration time is approximately1 to 6.5 s. The weld speed is 0 in this period. Fig. 14 and 15 shows the calculated temperature contours (top view) at different times during the penetration period. The figures graphically illustrate the temperature history of the workpiece during the pin penetration.

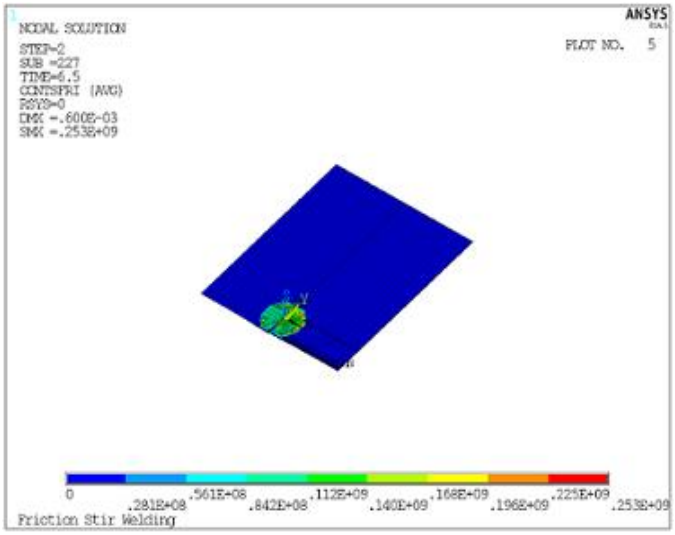

Fig. 9 Penetration period during load steps at 250 rpm

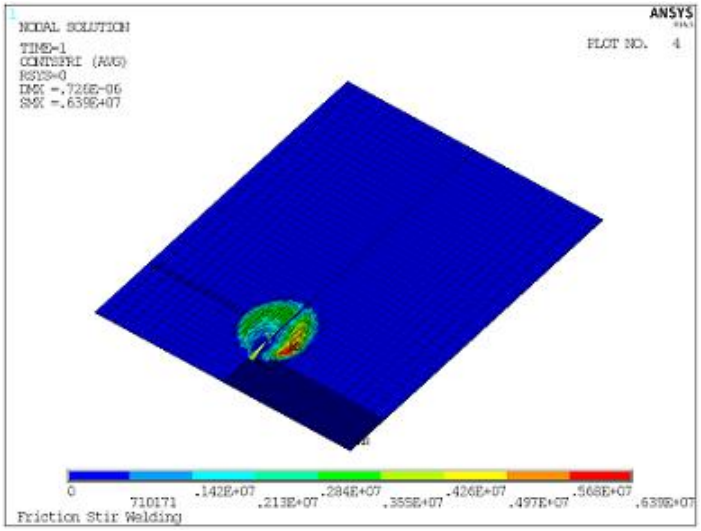

Fig. 10 Penetration period during load steps at 400 rpm

8. CONCLUSIONS

Modeling offers great potential for reducing experimental effort in development of welding parameters, tool design and many other areas and at the same time reduce cost and time. A simplified thermomechanical model was developed for friction stir welding for butt joint of 304L stainless steel. Based on kinematically compatible assumptions, this model predicts temperature contours in the welded zone between the shoulder and the workpiece. A successful comparison with different journal paper was carried out and the general tendencies for the influence of operational parameters were well predicted. The analysis of results concerning the contact conditions provides interesting data about the evolution of the relative sliding between the shoulder and the material to be welded and predict temperature distribution at different zones for different parameters.

The following conclusions can be drawn**: -**

(a) The virtual experimental data indicates that the temperature of weldment increases with increase in tool rotational speed while the temperature of weldment decreases with increase in welding speed. The result also indicates that the temperature at advanced side is higher than retract side.

(b) In this work a moving coordinate is in there so there are no moving heat source, therefore this model can be easily to applied heat-transfer process for both the tool and the workpiece during FSW.

(c) The computational results show that asymmetry of the temperature profiles around the tool because of the rotational and linear motion of the tool and asymmetry of heat generation around the tool pin surface.

REFERENCES

[1] Thomas WM, Nicholas ED, Needham JC, Murch MG, Templesmith P, Dawes CJ. Friction stir butt welding. US Patent 5,460,317; 1995.
[2] Dawes CJ, Thomas WM. Friction stir process welds aluminum alloys. Weld J 1996;75(3):41–5.
[3] Nicholas ED, Thomas WM. A review of friction processes for aerospace applications. Int J Mater Prod Technol1998;13(1/2):45–55.
[4] Thomas WM, Threadgill PL, Nicholas ED. Feasibility of friction stir welding steel. Sci Technol Weld Join1999;4(6):365–72.
[5] Thomas WM. Friction stir welding – recent developments Mater Sci Forum 2003;426–432:229–36.
[6] R.S. Mishra and Z.Y. Ma, —Friction stir welding and processing, Materials Science and Engineering, Vol. 1, R 50, pp. 1–78, 2005.
[7] Richard Johnson and Stephan Kallee, —Friction Stir Welding, Materials World, Vol. 7 no. 12, pp. 751-53, December 1999.
[8] W. Tang, X. Guo, J.C. McClure, L.E. Murr, A. Nunes, Heat input and temperature distribution in friction stir welding, J. Mater. Process. Manuf. Sci. 7 (1998) 163–172.
[9] J. Gould, Z. Feng, Heat flow model for friction stir welding of aluminum alloys, J. Mater. Process. Manuf. Sci. 7 (1998) 185–194.
[10] Y.J. Chao, X. Qi, Thermal and thermo-mechanical modeling of friction stir welding of aluminum alloy 6061-T6, J. Mater. Process. Manuf. Sci. 7 (1998) 215–233.
[11] Y.J. Chao, X. Qi, Heat transfer and thermo-mechanical modeling of friction stir joining of AA6061-T6 plates, in: Proceedings of the First International Symposium on Friction Stir Welding, Thousand Oaks, CA, USA, 1999.
[12] P. Colegrove, M. Pinter, D. Graham, T. Miller, Three dimensional flow and thermal modeling of the friction stir welding process, in: Proceedings of the Second International Symposium on Friction Stir Welding, Gothenburg, Sweden, June 26–28, 2000.
[13] O. Frigaard, O. Grong, O.T. Midling, A process model for friction stir welding of age hardening aluminum alloys, Metal. Mater. Transition A 32 (2001) 1189–1200.
[14] R. Talwar, B. Bolser, R. Lederich, J. Baumann, Friction stir welding of airframe structures, in: Proceedings of the Second International Symposium on Friction Stir Welding, Gothenburg, Sweden, June 26–28, 2000.
[15] Thermal modeling of friction stir welding in a moving coordinate system and its validation, M. Song, R. Kovacevic; 43 (2003) 605–615
[17] M.J. Russell, H.R. Shercliff, Analytical modeling of microstructure development in friction stir welding, Proceedings of the first International Symposium on Friction Stir Welding, Thousand Oaks, CA June 1999.
[18] A simple Eulerian thermomechanical modeling of friction stir welding,D. Jacquin, de Meester, Simar, D. Deloison, F. Montheillet, C. Desrayaud, 211 (2011) 57–65
[19] Zhang W, Roy GG, Elmer JW, Debroy T. Modeling of heat transfer and fluid flow during gas tungsten arc spot welding of low carbon steel. J Appl Phys 2003; 93:3020–33.
[20] Heat generation model for taper cylindrical pin profilein FSW, Vijay Shivaji Gadakha, Kumar Adepu; 2013-2(4):370–375
[21] Y.J. Chao, X. Zhu, X. Qi , a welding simulation code for the determination of transient and residual temperature, stress and distortion, in: S.N. Atluri, F.W. Brust (Eds.), Advances in Computational Engineering and Science, vol. II, Tech Science Press, Paledale, USA, 2000, pp. 1206–1211.
[22] G. Kohn, Laser-assisted friction stir welding, Welding Journal Feb (2002) 46–48.
[23] Zhu, X. K., and Y. J. Chao. "Numerical Simulation of Transient Temperature and Residual Stresses in Friction Stir Welding of 304L Stainless Steel." Journal of Materials Processing Technology. 146.2 (2004): 263-272.
[24] Chao, Y.J., X. Qi, and W. Tang. "Heat Transfer in Friction Stir Welding - Experimental and Numerical Studies." Journal of Manufacturing Science and Engineering-Transactions of the ASME. 125.1 (2003): 138-145.
[25] Prasanna, P., B. S. Rao, and G. K. Rao. "Finite Element Modeling for Maximum Temperature in Friction Stir Welding and its Validation." Journal of Advanced Manufacturing Technology. 51 (2010): 925-933